Planar cavity modes in void channel polymer photonic crystals

Michael James Ventura, Martin Straub, and Min Gu

Centre for Micro-Photonics and
Centre for Ultrahigh-bandwidth Devices for Optical Systems (CUDOS),
Faculty of Engineering and Industrial Sciences, Mail 38,
Swinburne University of Technology, P.O. Box 218, Hawthorn, Victoria 3122, Australia

mgu@swin.edu.au

Abstract: Planar dielectric microcavities embedded in woodpile void channel photonic crystals with stop bands in the stacking direction ranging from 4.3 to 4.8 μm in wavelength were generated by femtosecond-laser direct writing in a solid polymer. Infrared transmission spectra revealed fundamental and second-order modes crossing the stop gap region with a free spectral range of 430 nm on varying the microcavity size from 0.3 to 2.25 μm. Supercell calculations confirmed the cavity size dependence of highly localized cavity modes, whereas the angle of incidence was accounted for using a simple Fabry-Perot model.

©2005 Optical Society of America

OCIS codes: (220.4000) Microstructure fabrication; (050.2230) Fabry-Perot; (130.3130) Photonic integrated circuit; (999.9999) Photonic crystals.

References and links

1. E. Yablonovitch, "Inhibited spontaneous emission in solid-state physics and electronics," Phys. Rev. Lett. **58**, 2059-2062 (1987).
2. S. John, "Strong localization of photons in certain disordered dielectric superlattices," Phys. Rev. Lett. **58**, 2486-2489 (1987).
3. J. D. Joannopoulos, *Photonic crystals: modeling the flow of light* (Princeton University Press, U.S.A., 1995).
4. S. G. Johnson and J. D. Joannopoulos, *Photonic crystals, the road from theory to practice* (Kluwer Academic Publishers, U.S.A., 2002).
5. S. Y. Lin, V. M. Hietala, L. Wang, and E. D. Jones, "Highly dispersive photonic band-gap prism," Opt. Lett. **21**, 1771-1773 (1996).
6. H. Kosaka, T. Kawashima, A. Tomita, M. Notomi, T. Tamamura, T. Sato, and S. Kawakami, "Superprism phenomena in photonic crystals," Phys. Rev. B. **58**, R10096 (1998).
7. A. Sharkawy, S. Shi, and D. W. Prather, "Multichannel wavelength division multiplexing with photonic crystals," Appl. Opt. **40**, 2247-2252 (2001).
8. M. Koshiba, "Wavelength division multiplexing and demultiplexing with photonic crystal waveguide couplers," J. Lightwave Technology **19,**1970-1975 (2001).
9. B. Xu and H. Y. Ming, "Experimental observation of bistability and instability in a two-dimensional nonlinear optical superlattice," Phys. Rev. Lett. **71**, 3959-3962 (1993).
10. S. F. Mingaleev and Y. S. Kivshar, "Nonlinear transmission and light localization in photonic-crystal waveguides," J. Opt. Soc. Am. B **19**, 2241-2249 (2002).
11. M. Soljačić, C. Luo, J. D. Joannopoulos, and S. Fan, "Nonlinear photonic crystal microdevices for optical integration," Opt. Lett. **28**, 637-639 (2003).
12. N. Qi, E. Lidorikis, T. Rakich, S. G. Johnson, J. D. Joannopoulos, E. P. Ippen, and H. I. Smith, "A three-dimensional optical photonic crystal with designed point defects," Nature **429**, 538-542 (2004).
13. J. S. Foresi , P. R. Villeneuve, J. Ferrara, E. R. Thoen, G. Steinmeyer, S. Fan, J. D. Joannopoulos, L. C. Kimerling, H. I. Smith, and E. P. Ippen "Photonic-bandgap microcavities in optical waveguides," Nature **390**, 143-145 (1997).
14. S. Ogawa, M. Imada, S. Yoshimoto, M. Okano, and S. Noda, "Control of light emission by 3D photonic crystals," Science **305**, 227-229 (2004).

#6598 - $15.00 US Received 14 February 2005; revised 25 March 2005; accepted 28 March 2005
(C) 2005 OSA

15. M. M. Beaky, J. B. Burk, H. O. Everitt, M. A. Haider, and S. Venakides, "Two-dimensional photonic crystal Fabry-Perot resonators with lossy dielectrics," IEEE Trans. Microwave Theory Tech. **47**, 2085-2091 (1999).
16. H. B. Sun, V. Mizeikis, Y. Xu, S. Juodkazis, J. Y. Ye, S. Matsuo, and H. Misawa, "Microcavities in polymeric photonic crystals," Appl. Phys. Lett. **79**, 1-3 (2001).
17. K. Wostyn, X. Y. Zhao, G. de Schaetzen, L. Hellemans, N. Matsuda, K. Clays, and A. Persoons, "Insertion of a two-dimensional cavity into a self-assembled colloidal crystal," Langmuir **19**, 4465-4468 (2003).
18. O. Painter, R. K. Lee, A. Scherer, A. Yariv, J. D. O'Brien, P. D. Dapkus, and I. Kim, "Two-dimensional photonic band-gap defect mode laser," Science **284**, 1819-1821 (1999).
19. R. Ozaki, T. Matsui, M. Ozaki, and K. Yoshino, "Electrically color-tunable defect mode lasing in one-dimensional photonic band-gap system containing liquid crystal," Appl. Phys. Lett. **82**, 3593-3595 (2003).
20. S. H. Kim, H. Y. Ryu, H. G. Park, G. H. Kim, and Y. S. Choi, "Two-dimensional photonic crystal hexagonal waveguide ring laser," Appl. Phys. Lett. **81**, 2499-2501 (2002).
21. M. J. Ventura, M. Straub, and M. Gu, "Void channel microstructures in resin solids as an efficient way to infrared photonic crystals," Appl. Phys. Lett. **82**, 1649-1651 (2003).
22. M. Straub, M. Ventura, and M. Gu, "Multiple higher-order stop gaps in infrared polymer photonic crystals," Phys. Rev. Lett. **91**, 043901 (2003).
23. E. Özbay, A. Abeyta, G. Tuttle, M. Tringides, R. Biswas, C. T. Chan, C. M. Soukoulis, and K. M. Ho, "Measurement of a three-dimensional photonic band gap in a crystal structure made of dielectric rods," Phys. Rev. B. **50**, 1945-1948 (1994).
24. E. Hecht and A. Zajac, *Optics* (Addison-Wesley Publishing Company, U.S.A., 2002), Chap. 9.
25. H. Cao, D. B. Hall, J. M. Torkelson, and C. Q. Cao, "Large enhancement of second harmonic generation in polymer films by microcavities," Appl. Phys. Lett. **76**, 538-540 (2000).

1. Introduction

Ever increasing research effort was put into the fabrication and characterization of photonic crystals, since they were proposed independently by Yablonovitch [1] and John [2] over a decade ago. Exhibiting a photonic bandgap in which propagating electromagnetic modes cannot exist at all or only for certain directions or polarization states, photonic crystals allow for the highly efficient manipulation of light at wavelengths on the scale of their dielectric periodicity [3,4]. Along with numerous other attributes including abnormal dispersion [5,6] they are seen by many as the fundamental building blocks by which the optical integrated circuits of the future will be realized. The large variety of microdevices combined on such a photonic chip is based on specific deviations from the ideal lattice periodicity. Examples of such functional defects are waveguides with sharp bends [3,4], wavelength division multiplexers [7,8] and optical switches which rely on local nonlinearities [9-11]. Point defect microcavities may play an important role in these devices [7,10,11] and intense effort has been undertaken to study their electromagnetic modes [3,12-14]. Planar microcavities in photonic crystals [15-17] are another important defect category. Like point and line defects they hold particular promise upon combination with gain media and are key elements of photonic crystal microlasers [18-20], which may be integrated into the photonic chip. Microwave experiments with Fabry-Perot resonators in two-dimensional photonic crystals [15] revealed up to six cavity modes with quality factors on the order of 10^3 as well as characteristic spectral shifts with varying cavity size. Woodpile-type mid-infrared photonic crystals generated by two-photon photopolymerization [16] also showed signatures of defect modes upon removal of every second rod in their central layer. Recently, the insertion of a single layer of silica spheres of different size into a self-assembled colloidal photonic crystal allowed for the observation of a planar cavity mode shifting across the photonic stop gap in the visible spectral range [17].

In this article, we demonstrate the functionality of Fabry-Perot type planar microcavities with cavity spacings between 0.3 and 2.25 μm. The cavities were fabricated by femtosecond-laser direct writing of void channels in solid photopolymer resin [21,22]. Consistent with photonic eigenstate calculations, pronounced localized cavity modes were observed in the photonic stop gap region. With increasing cavity size two successive modes emerged from the air band, crossed the entire bandgap, and finally disappeared in the

#6598 - $15.00 US Received 14 February 2005; revised 25 March 2005; accepted 28 March 2005
(C) 2005 OSA

dielectric band along with characteristic changes in the mode profiles. Typical of Fabry-Perot etalons, an increasing angle of incidence resulted in a decline of the cavity mode wavelength.

2. Void channel woodpile photonic crystals: fabrication, characterization, and photonic band structure

Femtosecond-laser direct writing of submicron-size voids into a solid polymer host [21,22] is a single step process which allows for the generation of arbitary non-overlapping channel arrangements and requires no chemical post-processing. Controlled defects can be introduced at any location within the lattice geometry. The experimental set up is illustrated in Fig. 1(a). A femtosecond-pulsed Ti:sapphire laser beam (Mira 900-F; Coherent, Santa Clara, CA) operating at 810 nm passed through an optical parametric oscillator (OPO) with intracavity frequency doubler (Mira-OPO, Coherent; 1065-1265/545-625 nm) producing 580 nm laser light at a repetition rate of 76 MHz and a pulse width of 200 fs. A telescopic arrangement expanded and collimated the resultant beam uniformly illuminating the back aperture of an Olympus PlanApo 100x 1.4 numerical aperture (NA) oil immersion objective. A neutral density (ND) filter allowed for control of the fabrication power. The laser beam was focused into a pre-cured sample of Norland NOA63 optical adhesive sandwiched between two glass cover slips at a focal intensity of approximately 15 mW. The sample was affixed to a 200x200x200 µm x-y-z piezoelectric translation stage (P-562 with E-710 digital controller, Physik Instrumente, Waldbronn, Germany), which was operated at a scanning speed of 450 µm/s. The stage along with a shutter were both computer controlled and the entire fabrication process was monitored *in situ* by means of a charge-coupled device (CCD) camera collecting transmission illumination from a lamp situated beneath the sample.

Infrared transmission spectra of the fabricated photonic crystal structures were investigated using a Nicolet Nexus Fourier transform infrared (FTIR) spectrometer with Continuum infrared microscope (Thermo Nicolet, Madison, WI, U.S.A.). A mask consisting of a small pinhole was placed in front of a reflective 32x NA 0.65 objective (Reflechromat, Thermo Nicolet) which produced a hollow light cone varying from 18° to 41° [Fig. 1(b)]. With the mask in place a light cone of 5° in half angle was available and with the sample tilted normal incidence could be achieved. Although the mask reduced the effective numerical aperture to 0.09, the lateral sample size of 80 x 80 µm exceeded the Airy disk diameter and was large enough for optical probing.

The woodpile-style photonic crystal lattice was chosen due to its robust design by which many structural parameters can be varied. A computer-generated sketch of the void channel arrangement is shown in Fig. 1(c) and the corresponding Brillouin zone for this face-centred tetragonal (fct) lattice in Fig. 1(d). The lattice symmetry implies that electromagnetic modes in the stacking direction <001> are degenerate with respect to their polarization [23]. The photonic band structure was calculated using an iterative eigensolver program for a void channel woodpile lattice with a layer spacing of δz = 1.5 µm and an in-plane spacing of δx = 1.4 µm [Fig. 1(e)]. The corresponding fct unit cell dimensions were $a_{fct} = b_{fct} = \delta x\sqrt{2}$ and $c_{fct} = 4\delta z$ in the lateral and vertical directions, respectively. The primitive lattice vectors were $\mathbf{a_p} = (\delta x/\sqrt{2}, \delta x/\sqrt{2}, 0)$, $\mathbf{b_p} = (0, \delta x/\sqrt{2}, 2\delta z)$, $\mathbf{c_p} = (\delta x/\sqrt{2}, 0, 2\delta z)$ with a basis consisting of one channel in the direction of $\mathbf{a_p}$ at the origin and a perpendicular one at $\mathbf{b_p}/2$. The band diagram in Fig. 1(e) presents normalized mode frequencies using $a = |\mathbf{a_p}| = \delta x$ as well as the external (vacuum/air) wavelength λ and light speed c_0. Based on previous characterisation [22], void channels were taken to be embedded in a polymer host of effective refractive index 1.65 and to be elongated in the stacking direction with major and minor semiaxes of 500 nm and 330 nm, respectively. The band diagram reveals stop bands in the stacking direction Γ-X' between bands 2 and 3, 4 and 5, 6 and 7, as well as 8 and 9 (normalized frequencies at multiples of 0.15). Due to the low dielectric contrast, the small

#6598 - $15.00 US Received 14 February 2005; revised 25 March 2005; accepted 28 March 2005
(C) 2005 OSA

diameter of the void channels, and the strong deviation from the face-centred cubic (fcc) lattice geometry, a complete bandgap between bands 2 and 3 does not exist. Fig. 1(e) as well as more detailed photonic band calculations (not shown) demonstrate that, except for the gap between bands 4 and 5, the stop gaps exist only in narrow ranges of angles about the stacking direction. Therefore, the stop band at $\lambda = 4.56$ μm, which is indicated in Fig. 1(e) as a black bar, is called the main gap and was used for the investigation of planar microcavities.

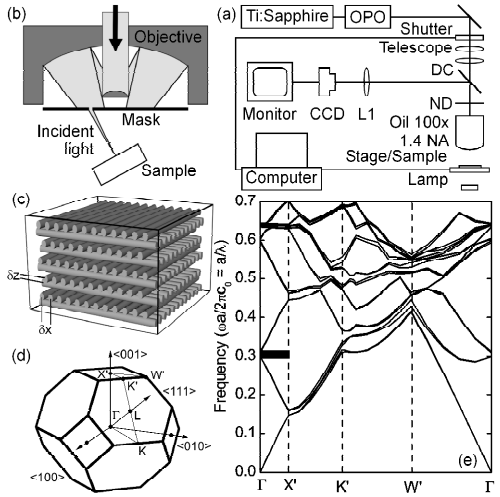

Fig. 1. (a) Setup for femtosecond-laser direct writing. OPO, optical parametric oscillator with intracavity frequency doubler; DC, dichroic mirror; ND, neutral density filter; Oil 100x 1.4 NA, oil immersion objective; CCD, charge-coupled device camera. (b) Infrared spectroscopy: reflective objective with a mask allowing for a light cone of 5° half angle. (c) Woodpile-type photonic crystal lattice consisting of elliptical void channels. (d) Brillouin zone of the face-centred tetragonal lattice. (e) Photonic band structure featuring a pronounced stop gap about the stacking direction Γ-X' at normalized frequency 0.30 (black bar).

3. Dependence of cavity modes on the defect layer size

Using the same experimental parameters, microcavities were fabricated at the centre of a twenty-four layer woodpile structure by the introduction of a displacement Δd of all layers beyond the twelfth [Fig. 2(a)]. Such a system is analogous to a Fabry-Perot etalon consisting of two parallel quarter-wave stacks [24], in which each layer of void channels contributes two quarter-wave layers of different average dielectric constant, one containing the channels and another one consisting entirely of cured resin. Related photonic band structures were calculated by setting up a cuboid-shaped supercell consisting of twenty-four layers of channels in the stacking direction with an additional spacing Δd between the twelfth and the thirteenth layer and one channel in both transverse directions (i.e. lateral size δx). Figure 2(b) shows the band diagram for a Δd of 2.1 μm, where the shaded areas denote frequencies outside the main photonic stop gap in the stacking direction. Within the stop gap a flat band at normalized frequency 0.306 (4.57 μm) demonstrates the existence of a localized defect mode. Bands below the lower gap edge at 0.289 (4.84 μm) are folded twelve times due to the supercell geometry chosen.

#6598 - $15.00 US Received 14 February 2005; revised 25 March 2005; accepted 28 March 2005
(C) 2005 OSA

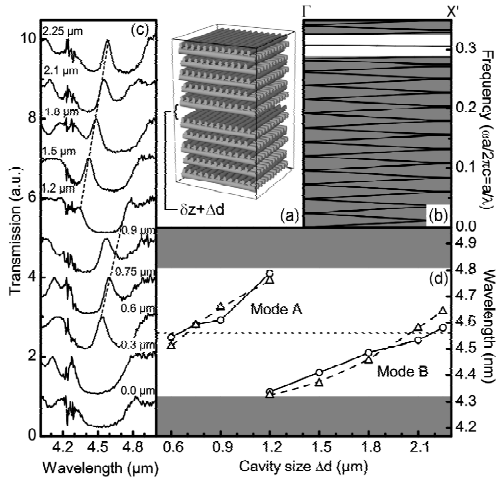

Fig. 2. (a) Sketch of a twenty four-layer void channel woodpile structure with a microcavity of size Δd in its centre. (b) Supercell calculation of photonic bands for a structure with a cavity size Δd of 2.1 µm. Shaded regions are frequencies outside the bandgap. The flat band within the bandgap denotes the cavity mode. (c) Infrared transmission spectra in the stacking direction for Δd from 0.3 to 2.25 µm. (d) Variation of experimental (circles) and calculated (triangles) cavity mode wavelengths with the cavity size.

A series of planar microcavities was fabricated with Δd ranging from 0.3 to 2.25 µm, as well as a reference structure without a defect. Figure 2(c) shows the resultant spectra. The dip in transmission centered on 4.5 µm is due to the main photonic stop gap of the woodpile photonic crystal lattice and agrees well with our calculations [Fig. 2(b)]. The striking feature which is apparent in all samples except the structure without a defect is a sharp peak within the stop gap region for Δd = 0.6 to 0.9 µm and again 1.5 to 2.25 µm constituting two successive cavity modes A and B, respectively. At a cavity size of 1.2 µm both modes are present simultaneously (Mode A at the upper gap edge in Fig. 2(b), Mode B at the lower one), although their appearance is less obvious as they are close to the gap edges.

Figure 2(d) compares the spectroscopy results (circles) with the eigenmode calculations (triangles). The shaded regions denote frequencies outside the bandgap, while the horizontal dotted line denotes the midgap frequency. The calculations reproduce the experimental results extremely well demonstrating the shift of both modes from the shorter to the longer-wavelength gap edge with increasing cavity size. As with typical quarter-wave stack Fabry-Perot filters our microcavities provide a first cavity mode at a cavity size of approximately a quarter-wave layer (Δd ≈ 0.75 µm) as well as a spacing between subsequent modes of 1.5 µm corresponding to half the light wavelength in the dielectric. Calculations confirm that a further increase of the cavity size or a (hypothetical) decrease to negative values by the same distance implying overlapping channels yields additional dielectric-type cavity modes. The coexistence of two modes at Δd = 1.2 µm is also confirmed theoretically allowing for bi-modal cavity operation with a free spectral range of 430 nm. The distributed feedback nature of the photonic crystal reflectors accounts for the order of magnitude smaller free spectral range compared to a simple Fabry-Perot etalon consisting of two reflective surfaces.

4. Angular dependence of cavity modes

Spectral measurements yielding an angular dependence further highlight the analogy to the Fabry-Perot etalon. For a cavity size of Δd = 0.6 µm over a range of angles of incidence of 0 - 10° a shift of the cavity mode to shorter wavelengths by approximately 20 nm was observed [Fig. 3(a) and 3(b)]. Taking into account the strong wavelength dependence of the phase shift

#6598 - $15.00 US Received 14 February 2005; revised 25 March 2005; accepted 28 March 2005
(C) 2005 OSA

upon reflection this result is consistent with the mathematical description of a simple Fabry-Perot etalon [24]:

$$m\lambda = 2dn\cos\theta_{FP} + (\phi/\pi)\lambda$$

with λ the (air/vacuum) light wavelength, d the effective cavity length, n the cavity refractive index, θ_{FP} the internal light propagation angle, and $\phi \approx \phi(\lambda_{midgap}) + \frac{\partial\phi(\lambda_{midgap})}{\partial\lambda}(\lambda - \lambda_{midgap})$ the phase shift upon reflection. With an effective cavity size $d = \lambda_{FP}/4 + \Delta d = 1.35$ μm (λ_{FP}: intracavity midgap wavelength) for the fundamental mode A, $\phi(\lambda_{midgap}) = 0.10\pi$ and $\frac{\partial\phi(\lambda_{midgap})}{\partial\lambda} = -0.21\pi/\mu m$ are obtained by a linear fit of λ against cos θ_{FP} [Fig. 3(c)]. The non-negligible phase shift may be explained by a minor deviation of the effective cavity size from a quarter-wave layer for $\Delta d = 0$.

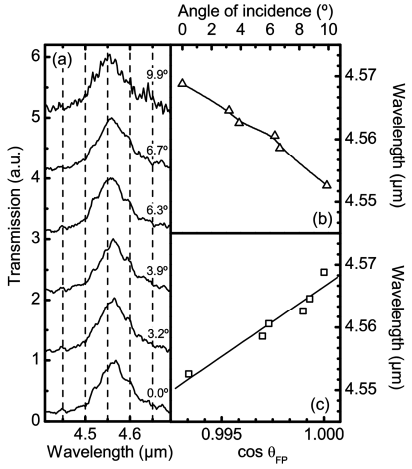

Fig. 3. With increasing angle of incidence the cavity modes shift to shorter wavelengths. (a) Infrared spectra for a cavity size of 0.6 μm. (b) Dependence of the mode A wavelength on the angle of incidence. (c) Linear fit using a simple Fabry-Perot model.

5. Cavity mode profiles

Supercell calculations not only reproduce the cavity size dependence of the mode wavelengths, but also demonstrate the degree of localization of the modes inside the cavity. Figure 4 shows the electromagnetic energy density of modes A (a-d) and B (e-h) of the woodpile-type lattice for Δd ranging from 0.4 to 2.5 μm in a vertical plane intersected by only one set of channels. The other set of channels is indicated by dashed lines in the outline of the lattice, which is overlaid on the profiles b and f. The color scale bar indicates the energy density from highest (red) to lowest (dark blue). The lower part of the figure plots the intensity along the stacking direction relative to the cavity position with horizontal planes containing void channels visualized by white areas (diagrams i, j). Mode A reveals a strong intensity maximum in the centre of the cavity, whereas mode B features two maxima with a central node. High intensity is confined to the cavity position and to a lesser extent to the adjacent dielectric. For both modes A and B modal confinement is strongest for cavity mode wavelengths near the midgap wavelength (b,c; f,g), whereas for mode wavelengths closer to the gap edges the modes extend deeper into the surrounding lattice (a,d; e,h). This influence of the photonic crystal reflectors on the cavity performance is also seen in the intensity plots,

#6598 - $15.00 US Received 14 February 2005; revised 25 March 2005; accepted 28 March 2005
(C) 2005 OSA

which demonstrate highest intensity in the cavity as well as the slowest decay of mode maxima at Δd = 0.8 μm and 2.1 μm for modes A and B, respectively.

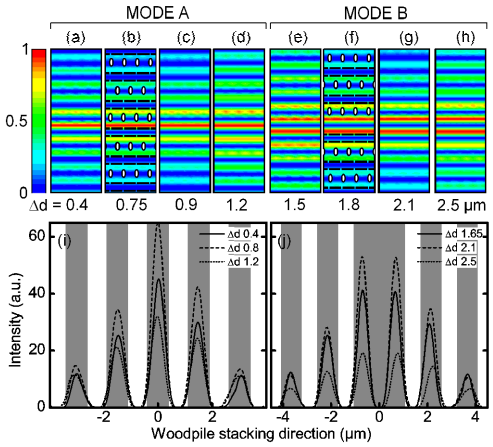

Fig. 4. (a-h) Energy density of modes A and B calculated in a vertical plane for a variety of cavity sizes. Overlaid in thin black on panels b and f is the outline of the crystal structure. (i,j) Mode profiles along the stacking direction. The grey areas correspond to horizontal planes entirely filled with dielectric. Close to the midgap wavelength (mode A: Δd = 0.8 μm, mode B: 2.1 μm) modes are localized more strongly within the cavity than close to the stop band edges.

6. Conclusions

In conclusion, high quality woodpile structures with the main photonic bandgap close to 4.5 μm were fabricated by femtosecond laser direct writing of void channels in polymer material, featuring planar cavities with sizes ranging from 0.3 to 2.25 μm. Infrared transmission measurements revealed pronounced cavity mode peaks within the photonic stop band yielding a characteristic dependence of the fundamental and second-order cavity mode wavelengths on the cavity size and the angle of incidence. Experimental results were explained by a quarter-wave stack and a simple reflective surface Fabry-Perot model as well as supercell calculations, which demonstrate the high degree of mode localization in the cavity. We emphasize that the efficient generation of such microcavities may find important applications, for example in the context of integrated microlasers, as they allow for the control of frequency, intensity, directionality and spectral width of light emission and even of nonlinear optical processes such as second harmonic generation [25].

Acknowledgments

This work was produced with the assistance of the Australian Research Council under the ARC Centres of Excellence program. CUDOS (the Centre for Ultrahigh-bandwidth Devices for Optical Systems) is an ARC Centre of Excellence.

#6598 - $15.00 US Received 14 February 2005; revised 25 March 2005; accepted 28 March 2005
(C) 2005 OSA